

Observation of vacuum-enhanced electron spin resonance of levitated nanodiamonds

Thai M. Hoang,¹ Jonghoon Ahn,² Jaehoon Bang,² and Tongcang Li^{1,2,3,*}

¹*Department of Physics and Astronomy, Purdue University, West Lafayette, IN 47907, USA*

²*School of Electrical and Computer Engineering,
Purdue University, West Lafayette, IN 47907, USA*

³*Birck Nanotechnology Center, Purdue University, West Lafayette, IN 47907, USA*

(Dated: July 22, 2022)

Electron spins of diamond nitrogen-vacancy (NV) centers are important quantum resources for nanoscale sensing and quantum information. Combining such NV spin systems with levitated optomechanical resonators will provide a hybrid quantum system for many novel applications. Here we optically levitate a nanodiamond and demonstrate electron spin control of its built-in NV centers in low vacuum. We observe that the strength of electron spin resonance (ESR) is enhanced when the air pressure is reduced. To better understand this novel system, we also investigate the effects of trap power and measure the absolute internal temperature of levitated nanodiamonds with ESR after calibration of the strain effect. Our results show that optical levitation of nanodiamonds in vacuum not only can improve the mechanical quality of its oscillation, but also enhance the ESR contrast, which pave the way towards a novel levitated spin-optomechanical system for studying macroscopic quantum mechanics. The results also indicate potential applications of NV centers in gas sensing.

INTRODUCTION

With electron spin states accessible by visible lasers and microwave radiation [1–3], diamond nitrogen-vacancy (NV) centers have broad applications in quantum information [4–6] and nanoscale sensing of magnetic field [7–9], temperature [10, 11], and beyond [12]. Combining such NV spin systems with mechanical resonators [13, 14] will provide a hybrid system with versatile functions. Recently, several authors proposed to levitate a nanodiamond with a built-in NV center in vacuum as a novel hybrid spin-optomechanical system for creating large quantum superposition states [15, 16], testing quantum wavefunction collapse models [15–17] and quantum gravity [18]. A levitated nanodiamond will also be an ultrasensitive mass spectrometer at room temperature [19]. These proposals are inspired by recent progresses in optomechanics of levitated pure dielectric (mainly silica) particles [20–24], which show optical levitation in vacuum can isolate the mechanical motion of a dielectric particle from the environment to improve the mechanical quality factor. Recently, nanodiamonds have been optically trapped in liquid [25, 26], atmospheric air [27] and low vacuum [28]. The next key step towards realizing these ambitious proposals [15, 16, 18, 19] is to control the NV electron spin of a levitated nanodiamond in a vacuum environment, which has not been demonstrated before.

Here we demonstrate the electron spin control and direct temperature measurement of NV centers in an optically levitated nanodiamond in low vacuum. To our surprise, the electron spin resonance (ESR) contrast of an optically levitated nanodiamond is enhanced in a vacuum environment. One would expect that the ESR signal of an optically levitated nanodiamond in vacuum to be

weaker than that in atmospheric air due to laser heating in vacuum. It has been previously observed that the ESR contrast of a NV center inside a bulk diamond decreases when the temperature increases from 300 K to 700 K [29]. We attribute the ESR enhancement in vacuum to the reduction of surrounding air molecules and surface contaminations which cause spin relaxation and decoherence. Our observation indicates a potential application of nanodiamond NV centers for gas sensing [30, 31]. To better understand this novel system, we investigate the effects of trapping laser on ESR and measure the absolute temperature of levitated nanodiamonds in vacuum with ESR [10, 29] after calibration of the strain effect [12]. The ability to remotely measure the internal temperature of a levitated nanodiamond will have applications in investigating nonequilibrium thermodynamics [32–34].

RESULTS

In our experiment, a nanodiamond with a diameter about 100 nm is optically trapped inside a vacuum chamber (Fig. 1a). We first launch a mixture of commercial nanodiamonds and water to the trapping region with an ultrasonic nebulizer. The water microdroplets evaporate and a nanodiamond will be captured by a tightly focused 500 mW 1550 nm laser beam after waiting for a few minutes (see Methods). After a nanodiamond is captured, we evacuate the air in the chamber by a turbomolecular pump. A trapped nanodiamond will eventually be lost when the air pressure is below a critical value, which is a few Torr for commercial nanodiamonds that we used (see Methods).

Effects of trapping laser on nanodiamond electron spin resonance. For an optically levitated nanodiamond, one needs to consider effects of the trapping

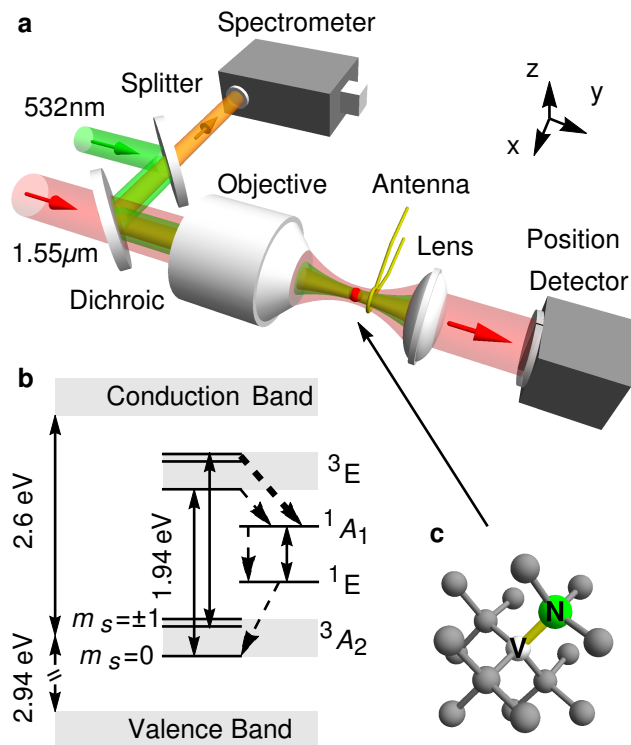


FIG. 1. **Schematic of the experiment.** **a** A nanodiamond (red sphere) is trapped inside the vacuum chamber using an optical tweezers formed by a 1550 nm laser and an objective lens. The position detector monitors its center-of-mass motion. The NV centers are optically excited by a 532 nm beam guided by a beam splitter and a long-pass dichroic mirror. The fluorescent signal (orange beam) of the NV centers is detected by a spectrometer with an EMCCD camera. Electron spins are controlled by microwave delivered by an antenna (see Methods). **b**, Energy levels of a NV^- center. Solid arrows represent radiative transitions while dashed ones represent nonradiative transitions. **c**, Molecular structure of a NV center. Carbon atoms are shown in gray spheres, the lattice vacancy is labeled by a white ‘V’ sphere and the nitrogen atom is labeled by a green ‘N’ sphere. Each nanodiamond has about 500 NV centers.

laser while studying its NV centers. We investigate this effect by measuring the fluorescence spectra and ESR spectra at different trapping powers (Fig. 2). We excite the trapped nanodiamond with a 532 nm laser and collect its fluorescent signal by a spectrometer with an EMCCD (electron multiplying charge coupled device) camera with a single-photon sensitivity. To study the ESR, we excite the electron spin states by microwave radiation delivered by a coplanar waveguide antenna (see Methods). The normalized fluorescence signal I_{PL} of the ESR spectrum is the ratio of total fluorescence count with and without the microwave excitation. The resonance peaks of electron spin transition occur at the microwave frequencies of minimum I_{PL} . The ESR contrast is defined as $1 - I_{PL}$.

As shown in Fig. 2a,b, both the fluorescent signal and

the ESR contrast decrease when the trapping power increases. To understand these phenomena, we need to consider two primary effects associated with the trapping laser: heating [35] and photo-induced ionization when a 532 nm laser is also present [36]. Since the absorption of the trapping laser increases temperature, a higher trapping power leads to a higher temperature of the nanodiamond (Fig. 2c). The visible fluorescent signal comes from the radiative decay transition ${}^3E \rightarrow {}^3A_2$. There is also a competing process that the excited state 3E may relax to the ground state 3A_2 through nonradiative process with metastable states 1E and 1A_1 (Fig. 1b). Since high temperature enhances the nonradiative decay [29], it weakens the visible fluorescence strength (Fig. 2a) and the ESR contrast (Fig. 2b).

The internal temperature of nanodiamond is obtained from a double Gaussian fit of the ESR data [10, 29] (see Methods). As shown in Fig. 2c, the temperature of each nanodiamond increases linearly with the trapping power (within the range of measured data), although of the slope of each line is different. We can use this linear dependence relation to determine the internal strain of each trapped nanodiamond. The internal strain can shift of the ESR spectrum in a range of several MHz depending on each nanodiamond [37]. This could lead to an overestimation or underestimation of the nanodiamond temperature by tens of kelvins if we do not consider the internal strain. Since we know the internal temperature of the nanodiamond is at room temperature when the power of the trapping laser is zero, we can treat the internal strain of each nanodiamond as a fitting parameter such that each temperature-trap power line in Fig. 2c intersects the vertical axis at 296 K when the laser power is zero. So we can take into account the effect of strain on the temperature measurement.

Besides heating, the 1550 nm trapping laser can cause photo-induced ionization of NV^- to NV^0 when the 532 nm laser is on [36, 38–40]. As shown in Fig. 1b, the 532 nm laser excites the NV centers from the ground state 3A_2 to the excited state 3E . Since the separation between the excited state and the conduction band is 0.67 eV (corresponding to a vacuum wavelength of 1880 nm) [36], the 1550 nm trapping beam can excite electrons from the excited state 3E to the conduction band and consequently ionize NV^- to NV^0 . Because high trapping power increases the ionization rate from NV^- to NV^0 , the fluorescence signal from NV^- will be reduced as seen in Fig. 2a. Similar effects have been observed for laser wavelength 1064 nm and below [27, 35–40]. We note that the 1550 nm laser is better than a 1064 nm laser as we can observe strong fluorescence signal at 500 mW, while a 100 mW 1064 nm laser quenches the fluorescence [27, 37]. The ionization not only reduces the fluorescence strength, but also lessens the ESR contrast. When the recombination of NV^0 to NV^- occurs [36], the probability of NV^0 ending up in $|m_s = 0\rangle$ state will be 1/3 since the thermal

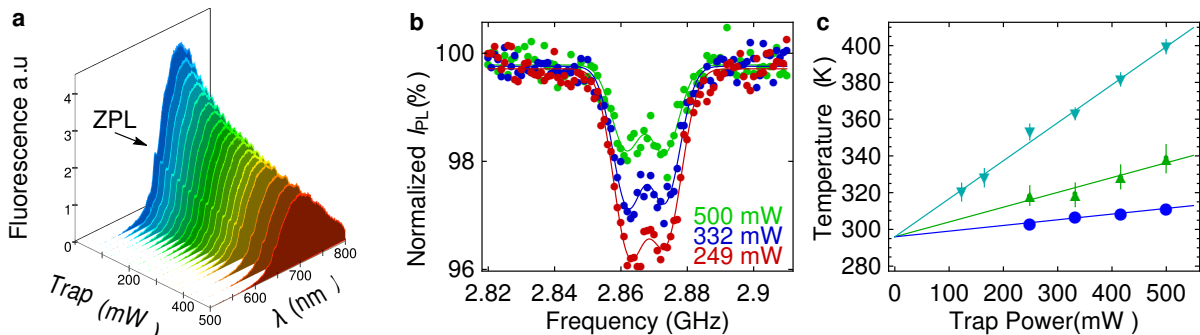


FIG. 2. **Effects of optical trapping power.** **a**, The fluorescence strength increases by about 2.5 times when the power of the trapping laser is reduced from 500 mW to 60 mW. The zero phonon line (ZPL) is indicated by the arrow. The nanodiamond is excited with a $260 \mu\text{W}$ green laser. **b**, Electron spin resonance (ESR) spectra of NV^- centers at different trapping powers. Normalized I_{PL} is the ratio of the total fluorescence count with and without microwave excitation. The data was taken with a green laser of $30 \mu\text{W}$ and each ESR scan takes about 30 minutes to achieve a high signal-to-noise ratio. **c**, At the initial trapping power of 500 mW, the internal temperature of the nanodiamond ranges between 300-400 K depending on individual nanodiamond. When the trapping power reduces, the internal temperature of the nanodiamond approaches the room temperature (296 K). Temperatures are extracted from the double Gaussian fits of the ESR spectra (see Method). Each marker shape represents a different nanodiamond. Data are acquired at atmospheric pressure. a.u. denotes an arbitrary unit.

energy in nanodiamond is larger than the energy splitting of $|m_s = 0, \pm 1\rangle$ states. Thus the ionization due to trapping laser will reduce the overall population of $m_s = 0$ below the 84% level of the unperturbed nanodiamond [41], and reduces the ESR contrast.

Vacuum-enhanced electron spin resonance.

Since nanodiamond temperature increases in vacuum, the ESR spectrum shifts to the left as shown in Fig. 3a. From atmospheric pressure to 31 Torr, the diamond temperature can rise from 300 K to above 450 K (Fig. 3b). When the temperature rises in vacuum, one would expect the ESR contrast to decrease. Counter intuitively, the data show that the ESR contrasts of levitated nanodiamonds increase by more than a factor of 2 when the pressure is decreased from atmospheric pressure to 31 Torr (Fig. 3a,c). This important phenomenon has not been observed before since the ESR of a levitated nanodiamond has not been studied in a vacuum environment prior to our work. The latest relevant work reported the ESR of a levitated nanodiamond in atmospheric air [28], but not in vacuum.

To understand this phenomenon, we need to consider two primary changes related to vacuum: the nanodiamond temperature and the concentration of surrounding gases. A former study shows that the ESR contrast of a NV center inside a bulk diamond decreases by about 7% when the temperature is increased from 300 K to 450 K [29]. So the phonon effect of high temperature can not explain our result that the ESR contrast increases by more than a factor of 2 in vacuum. The increasing of ESR contrast should be a result of the reduction of the concentration of surrounding gases and surface contamination in vacuum. There are a few studies on the spin relaxation and decoherence due to ion spins in liq-

uid and nearby surface [30, 31, 42]. Magnetic fluctuation from spin impurities [31] and surrounding gases can cause spin relaxation and decoherence, and consequently reduces the ESR contrast. In a vacuum environment, surrounding gas molecules are eliminated and many absorbed molecules on the nanodiamond surface evaporate. An increase of temperature also helps the evaporation of absorbed molecules. So the external spin relaxation and decoherence sources are reduced and the ESR signal can be improved.

To verify that the increase in ESR contrast is primarily because of the reduction of surrounding and absorbed air molecules instead of a permanent change of the nanodiamond, we performed an experiment in which the chamber was first pumped from atmospheric pressure to 74 Torr, and then brought back to atmospheric pressure. The contrast at the later atmospheric pressure is slightly higher than the initial atmospheric pressure (red square markers in Fig. 3c), but significantly smaller than the ESR contrast at low pressure. The slight increase of the ESR contrast at the later atmospheric pressure can be explained by the purification of the nanodiamond after exposed to vacuum. The surface contamination of the nanodiamond can evaporate or be oxidized when the temperature of the nanodiamond reaches above 400 K in low vacuum [43, 44]. This purification reduces the background fluorescence signal from the impurity and increases the ESR contrast. If the nanodiamond is permanently changed, one would expect the nanodiamond maintaining a high ESR contrast when the pressure is brought back to atmospheric level from 74 Torr. However, the data indicate that the ESR contrast at later atmospheric pressure is lower than that at 74 Torr. In addition to the ESR contrast, we also monitored the total fluorescence counts during the experiment. The total fluorescence counts at

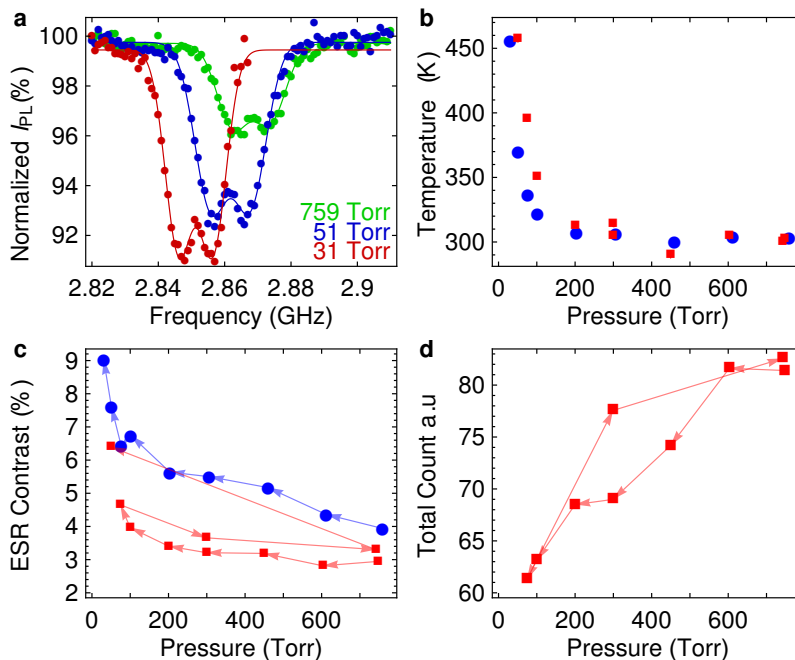


FIG. 3. **Vacuum-enhanced electron spin resonance.** **a**, ESR spectra of a levitated nanodiamond at different pressures. Each ESR scan takes approximately 30 minutes to achieve a high signal-to-noise ratio. The peaks of the ESR spectra shift in vacuum due to the thermal effect. **b**, The measured temperature of two different nanodiamonds as a function of air pressure. From atmospheric pressure to low vacuum, their temperatures change from 300 K to 450 K and beyond. The errorbar of temperature measurement is smaller than the marker size. Each marker shape represents a different nanodiamond. **c**, The maximum contrast of each ESR spectrum increases as the air pressure decreases. Arrows of the lines indicate the time order of the experiment. **d**, The total fluorescence count as a function of air pressure. The time order of data is indicated by arrows. The fluorescence strength is almost the same at atmospheric pressure before and after going to 75 Torr. The trapping power for each nanodiamond is always held constant. a.u. denotes an arbitrary unit.

initial atmospheric pressure and later atmospheric pressure are almost the same (Fig. 3d). Combining the ESR and fluorescence data together, we conclude that there is no significant change of the nanodiamond after exposed to low vacuum. Therefore, the reduction of the surrounding and absorbed air molecules is the primary source for the ESR enhancement. One candidate for these air molecules is the paramagnetic oxygen molecules (O_2) in air which has a ground state with net electron spin =1. A former experiment has observed that 1.5 mmol/L of O_2 dissolved in water reduces the spin relaxation time T_1 of diamond NV centers [31]. The O_2 concentration in air at atmospheric pressure is about 9.4 mmol/L, so we expect it will affect the ESR of a levitated nanodiamond as well. The absorbed O_2 molecules on the nanodiamond surface can also affect the ESR. This can at least partially explain the increase of ESR when the air pressure is reduced, and indicate potential applications of diamond NV centers in gas sensing. More detailed studies are necessary to fully understand this important phenomenon.

DISCUSSION

In this paper, we optically levitate a nanodiamond and demonstrate electron spin control of its built-in NV centers in low vacuum. We observed that the ESR contrast of NV centers increases when the air pressure decreases. We attribute this ESR enhancement in vacuum mainly to the reduction of surrounding and absorbed air molecules such as paramagnetic oxygen [30, 31] that cause spin relaxation and decoherence. While more detailed studies are required to fully understand this phenomenon, it suggests a potential application of nanodiamond NV centers for gas sensing. The vacuum-enhanced ESR can also improve the sensitivity of other NV center devices such as nanodiamond magnetic/electric field sensors where the NV centers are near the diamond surfaces. We also study the effects of trapping laser and measure the absolute internal temperature of the levitated nanodiamond in vacuum to better understand this novel system. The results show that the internal temperature of an optically levitated nanodiamond increases significantly in low vacuum. This is because the commercial nanodiamonds used in this work are not pure and have large optical absorption. Better nanodiamond samples with negligible absorption

[45] at the trapping wavelength are required to be optically trapped in high vacuum.

METHODS

Experimental setup. A mixture of nanodiamonds (Adamas ND-NV-100nm-COOH) and water at density about 30 $\mu\text{g}/\text{ml}$ is launched into vacuum chamber using a Mabis supersonic nebulizer for optical trapping. A nanodiamond is captured and trapped by a 1550 nm laser beam at the focus of a NA=0.85 infrared objective lens (Fig. 1a). The position detector monitors [32] the center of mass motion of the nanodiamond using the trapping beam after exiting the vacuum chamber. The NV centers are optically excited by a 532 nm laser beam guided by a beam splitter and a 950 nm long pass dichroic mirror. The fluorescence signal of the NV centers are detected by an Andor spectrometer and a Newton EMCCD (electron multiplying charge coupled device) camera. The electron spin of NV centers are controlled using a microwave antenna [25] at a distance of 0.5 mm from the nanodiamond.

Optical levitation of a nanodiamond with built-in NV centers in low vacuum. To verify the trapped nanodiamond (Fig. 4a) has NV centers, we excite the particle with a 532 nm green laser beam and analyze the fluorescence signal using a spectrometer with an EMCCD (Fig. 1a). One unique signature of NV^- center is the zero phonon line (ZPL) around 637 nm due to the 1.94 eV transition between the 3A_2 ground state and the 3E excited state as depicted in Fig. 1b [10, 36]. At room temperature, the visible fluorescence spectrum covers from 600 – 800 nm due to thermal phonon broadening. In Fig. 4b, the fluorescence spectrum indicates a ZPL at 640 nm. This small shift of ZPL from 637 nm is because of temperature effect [3, 11, 46].

We observe that the visible fluorescent strength of levitated NV centers decreases and the ZPL becomes weaker in vacuum due to thermal effect (Fig. 4b). When the air pressure decreases, the nanodiamond temperature rises because the cooling rate from air molecules reduces while the heating from the trapping laser remains the same. The visible fluorescent strength of NV centers is determined by the competition between the radiative decay and the nonradiative decay from the excited 3E triplet state [10, 29, 47, 48]. A high temperature can enhance the nonradiative process [29], leading to a drop of the fluorescent signal. This observation agrees with other recent experiments of NV centers performed at high temperature [29, 49].

Besides optical properties of NV^- centers, we also monitor the center-of-mass motion (CMM) of a trapped nanodiamond using the x -axis position detector [32]. At atmospheric pressure, Brownian motion due to collisions with air molecules predominates the harmonics oscillation due to the trapping potential. In low vacuum, the

harmonic motion dominates the CMM. As a result, a resonant peak (≈ 100 kHz) appears in the spectrum of power spectral density (PSD) of the CMM at low pressure (Fig. 4c). Fitting the PSD data to theory (see Eq. 1) reveals useful information about the optomechanics system [50], including trapping frequency Ω_0 and viscous damping factor due to air molecules Γ_0 . The trapping frequency $\Omega_0/2\pi$ is about 100 kHz and viscosity damping coefficient $\Gamma_0/2\pi$ goes from about 500 kHz at atmospheric pressure to about 40 kHz at 31 Torr. From the fitting parameter $\Gamma_0/2\pi$, the hydrodynamic diameter of nanodiamond, $r = 94 \pm 7$ nm (see Eq. 2), remains constant for over 30 minutes (Fig. 4d). This result is consistent with the manufacture specification size of 100 nm. In fact, we observed that a single nanodiamond remains in the trap for many hours at atmospheric pressure and in low vacuum. A trapped nanodiamond will be lost, however, when the air pressure is below a critical value. Fig. 4f shows a nanodiamond is lost when the pressure is reduced to 9 Torr. We also observed some nanodiamonds trapped at slightly lower pressures.

Combining the fluorescence signal and center-of-mass motion together provides an insight into the loss mechanism of levitated nanodiamonds in vacuum. As shown in Fig. 4e, a levitated nanodiamond is lost after being held at 31 Torr for 17 minutes. The total count of the fluorescence signal first decreases gradually and then drops rapidly within the last 60 seconds before the nanodiamond is lost (Fig. 4e). Based on the fluorescence signal alone, one might conclude that the nanodiamond is gradually burned in residual air in the vacuum chamber. However, the viscous damping factor $\Gamma_0/2\pi$ which is related to the particle size (see Eq. 2) is fairly constant at 31 Torr. So the size of the nanodiamond does not change significantly before it is lost. This is consistent with the internal temperature of the nanodiamond measured by the ESR which will be discussed later. For the nanodiamond shown in (Fig. 4e), its internal temperature is about 450 K (177 °C). According to a former investigation, the size reduction speed of nanodiamond due to air oxidization at atmospheric pressure is about 1 nm/hour at 770 K. At 450 K, the size reduction of a nanodiamond should be negligible, especially because the oxygen pressure is low in low vacuum. So the loss of a trapped nanodiamond is unlikely due to oxidization. Instead, when the temperature of the nanodiamond and surrounding air increases, the amplitude of the Brownian motion also increases [33]. A larger vibration amplitude can lead to a decrease of the fluorescence signal when nanodiamond randomly walks away the trapping region (overlapping with the focus of the visible imaging system). Moreover, the scattering force of the optical tweezers is nonconservative, it can pump energy into the nanodiamond. If the particle moves in loops due to its irregular shape, it can escape from the trap. Though, more studies are required to further clarify the loss mechanism.

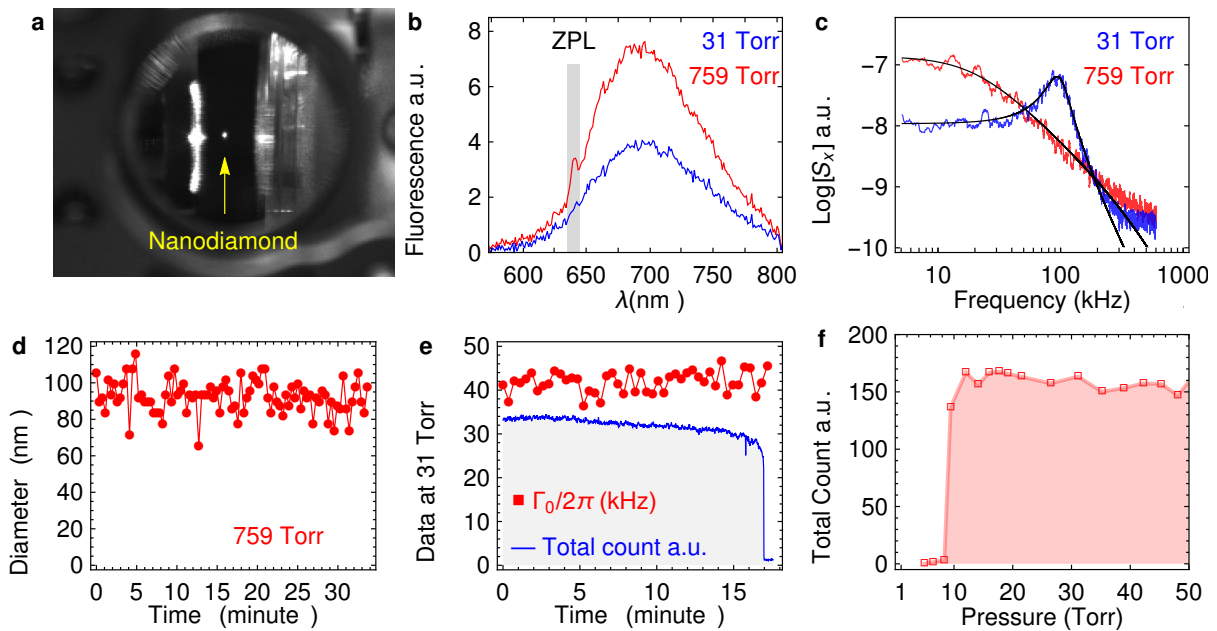


FIG. 4. **A levitated nanodiamond in low vacuum.** **a**, An image of an optically levitated nanodiamond (bright white spot) inside the vacuum chamber. **b**, Typical fluorescence spectra at atmospheric pressure (759 torr) and in low vacuum (31 Torr). The nanodiamond is excited with a $30 \mu W$ green laser. The zero phonon line of NV^- is visible near 640 nm. **c**, Power spectral density of the center-of-mass motion of a nanodiamond trapped at two different pressures (red: 759 torr; blue: 31 torr). A resonant peak appears in low vacuum. The solid black curves are theoretical fits (see Eq. 1). **d**, The hydrodynamic diameter of a trapped nanodiamond calculated from the measured viscosity damping Γ_0 (see Eq. 2). **e**, The viscous damping factor Γ_0 and total fluorescence count of a levitated nanodiamond at 31 Torr. The nanodiamond is lost at the right side of this figure. The Γ_0 is fairly constant, suggesting there is no change in the particle size before its loss. The same nanodiamond is used in figures **b**, **c**, **d** and **e**. **f**, Total fluorescence count of an optically trapped nanodiamond when the chamber is pumped to vacuum. The nanodiamond is lost at 9 Torr. a.u. denotes an arbitrary unit.

Center of mass motion calibration. When the nanodiamond is at the thermal equilibrium, the power spectra density (PSD) of nanodiamond CMM is given by [51]

$$S_x(\omega) = S_0 \frac{\Gamma_0}{(\Omega_x^2 - \omega^2)^2 - \omega^2 \Gamma_0^2} \quad (1)$$

here $S_0 = 2k_B T/m$, k_B is the Boltzmann constant, T is the air temperature, m is the nanodiamond mass, Γ_0 is the viscous damping factor due to the air, Ω_x is the trapping frequency in the x -axis, and ω is the observation frequency. Fitting the CMM power spectral density data in Fig. 4c to Eq. 1, one can extract three fitting parameters S_0 , Γ_0 , and Ω_x . In general, the fit works best when the ω_x is comparable to Γ_0 or when pressure is below 300 Torr. The trapping frequency depends on the laser trapping power. Since the refractive index of air is 1.0027, similar to vacuum, the trapping potential in air should be the same as in vacuum. Moreover, the trapping frequency Ω_x does not change much from 300 Torr to 10 Torr according to the data. Therefore, the trapping frequency is presumably constant.

Particle size calculation. Since it is difficult (and not important) to know the exact shape and size of the nanodiamond (which can be irregular), we estimate its

hydrodynamic size from the viscous damping factor as [23, 52]

$$\Gamma_0 = \frac{6\pi\eta r}{\rho(4/3\pi r^3)} \frac{0.619}{0.619 + Kn} (1 + c_K) \quad (2)$$

where η is the dynamic viscosity coefficient of the air, r is the hydrodynamic radius of the nanodiamond, $Kn = s/r$ is the Knudsen number with s being the mean free path of air molecules, and $c_K = 0.31Kn/(0.785 + 1.152Kn + Kn^2)$. The mean free path is linearly dependent on the viscosity as [52]

$$s = \frac{\eta}{P} \sqrt{\frac{\pi k_B T}{2m_{air}}} \quad (3)$$

here P is the pressure and m_{air} is the mass of air molecule. In 1866, Maxwell demonstrated that the viscosity of air maintains constant from atmospheric pressure down to a few Torr [53]. At atmospheric pressure, the nanodiamond in Fig. 4d (≈ 300 K) is presumably in thermal equilibrium with air molecules. The temperature dependence of the viscosity can be calculated using Sutherland's formula [54] which yields $\eta \approx 18.52 \times 10^{-6}$ (Pa s) and $s \approx 67$ nm at room temperature (296 K). The viscous damping factor is $\Gamma_0 \approx 500$ kHz obtained from the power spectral density fit of Fig. 4c with Eq. 1.

Solving for r in Eq. 2, we obtain the nanodiamond diameter of 94 ± 7 nm while monitoring the particle size for over 30 minutes (Fig. 4d). At low vacuum, nanodiamond is not in thermal equilibrium with surrounding gases due to its high temperature, Eq. 2 is not suitable to calculate the particle size.

ESR Technique. The ESR experiments was conducted using an optically detected magnetic resonance (ODMR) technique [3, 55]. We employed a similar microwave antenna design and the microwave lock-in technique described in Refs. [25]. To obtain the ESR signal, the electron spin states are excited $|m_s = 0\rangle \leftrightarrow |m_s = \pm 1\rangle$ by microwave pulses. For a given frequency, the antenna delivers a sequence of 500 ms alternative on/off microwave pulses to control the electron spin of NV centers. When the microwave pulse is on, the NV ground spin state $|m_s = 0\rangle$ is excited to $|m_s = \pm 1\rangle$, and vice versa. At the same time, the visible fluorescence spectrum of the diamond is acquired using the spectrometer (Fig. 1a). Since the visible fluorescence signal of $|m_s = \pm 1\rangle$ is weaker than $|m_s = 0\rangle$ state, the ESR spectrum is the plot of the normalized I_{PL} measurements. The normalized fluorescence signal I_{PL} of ESR spectrum is the ratio of total fluorescence counts with and without microwave excitation, where the resonance peaks occur at the frequencies of minimum I_{PL} .

Diamond temperature The zero-field Hamiltonian of NV center is written as [8]

$$\mathcal{H} = DS_z^2 + E(S_x^2 - S_y^2) \quad (4)$$

Here D is the energy splitting between spin ground state $|m_s = 0\rangle$ and $|m_s = \pm 1\rangle$, and E is the splitting between $|m_s = \pm 1\rangle$ due to the broken axial symmetry of the NV center caused by the strain effect [3, 56]. This Hamiltonian results in a double peak resonance spectrum as seen in Fig. 2b where D is center of the double peaks, and E is the separation between two resonance peaks. The parameter E is different for each unique NV center. Overall we observe a separation $2E \sim 10$ MHz which is consistent with early measurements in bulk diamond [3, 10]. Since the ambient magnetic field was measured to be 600 mG using a commercial magnetometer, the separation between two resonance peaks is mainly contributed by the zero-field parameter E . The zero-field splitting parameter D depends on temperature as [29]

$$D(T) = a_0 + a_1T + a_2T^2 + a_3T^3 + \Delta_{pressure} + \Delta_{strain} \quad (5)$$

here $a_0 = 2.8697$ GHz, $a_1 = 9.7 \times 10^{-5}$ GHz/K, $a_2 = -3.7 \times 10^{-7}$ GHz/K², $a_3 = 1.7 \times 10^{-10}$ GHz/K³, $\Delta_{pressure} = 1.5$ kHz/bar is the pressure dependence shift [57], and Δ_{strain} is the internal strain effect depending on the particle.

Each individual nanodiamond has a different internal strain Δ_{strain} about a few MHz. This could lead to an

uncertainty of tens of kelvins in measuring the absolute temperature if Δ_{strain} is neglected. From atmospheric pressure to 1 Torr, the shift due to pressure is about 1.5 kHz, equivalent to changing nanodiamond temperature by 20 mK, which is negligible compared to the thermal shift. One can solve for temperatures T from $D(T)$ in Eq. 5 using the parameters D obtained from the double Gaussian fit of ESR spectra [10, 25]. Since we know the internal temperature of the nanodiamond is at room temperature (296 K) when there is no trapping laser, the linear fit in Fig. 2c should intersect the vertical axis at 296 K when the laser power is zero. From this known temperature at the limit of zero trapping power, we determine the internal strain Δ_{strain} of each individual nanodiamond.

Acknowledgements We acknowledge the support from Purdue University. We would like to thank helpful discussions with F. Robicieux, C. Zu, Z. Yin, N. Zhao, M. Y. Shalaginov, and V. M. Shalaev.

Author Contributions. T.M.H. and T.L. conceived and designed the project, and analyzed the data. T.M.H., J.A, J.B. built the experimental apparatus. T.M.H. performed measurements. T.L. supervised the work. All authors co-wrote the paper.

-
- * Correspondence and requests for materials should be addressed to T.L. (email: tcli@purdue.edu).
- [1] Clark, C. and Norris, C. Photoluminescence associated with the 1.673, 1.944 and 2.498 eV centres in diamond. *Journal of Physics C: Solid State Physics* **4**(14), 2223 (1971).
 - [2] Loubser, J. and van Wyk, J. Electron spin resonance in the study of diamond. *Reports on Progress in Physics* **41**(8), 1201 (1978).
 - [3] Gruber, A., Dräbenstedt, A., Tietz, C., Fleury, L., Wrachtrup, J., and Von Borczyskowski, C. Scanning confocal optical microscopy and magnetic resonance on single defect centers. *Science* **276**(5321), 2012–2014 (1997).
 - [4] Neumann, P., Mizuochi, N., Rempp, F., Hemmer, P., Watanabe, H., Yamasaki, S., Jacques, V., Gaebel, T., Jelezko, F., and Wrachtrup, J. Multipartite entanglement among single spins in diamond. *Science* **320**(5881), 1326–1329 (2008).
 - [5] Togan, E., Chu, Y., Trifonov, A., Jiang, L., Maze, J., Childress, L., Dutt, M. G., Sørensen, A. S., Hemmer, P., Zibrov, A., et al. Quantum entanglement between an optical photon and a solid-state spin qubit. *Nature* **466**(7307), 730–734 (2010).
 - [6] Neumann, P., Kolesov, R., Naydenov, B., Beck, J., Rempp, F., Steiner, M., Jacques, V., Balasubramanian, G., Markham, M., Twitchen, D., et al. Quantum register based on coupled electron spins in a room-temperature solid. *Nature Physics* **6**(4), 249–253 (2010).
 - [7] Degen, C. Scanning magnetic field microscope with a diamond single-spin sensor. *Applied Physics Letters* **92**(24), 243111 (2008).
 - [8] Balasubramanian, G., Chan, I., Kolesov, R., Al-Hmoud, M., Tisler, J., Shin, C., Kim, C., Wojcik, A., Hemmer, P. R., Krueger, A., et al. Nanoscale imaging magnetometry with diamond spins under ambient conditions. *Nature* **455**(7213), 648–651 (2008).
 - [9] Taylor, J., Cappellaro, P., Childress, L., Jiang, L., Budker, D., Hemmer, P., Yacoby, A., Walsworth, R., and Lukin, M. High-sensitivity diamond magnetometer with nanoscale resolution. *Nature Physics* **4**(10), 810–816 (2008).
 - [10] Acosta, V., Bauch, E., Ledbetter, M., Waxman, A., Bouchard, L.-S., and Budker, D. Temperature dependence of the nitrogen-vacancy magnetic resonance in diamond. *Physical review letters* **104**(7), 070801 (2010).
 - [11] Chen, X.-D., Dong, C.-H., Sun, F.-W., Zou, C.-L., Cui, J.-M., Han, Z.-F., and Guo, G.-C. Temperature dependent energy level shifts of nitrogen-vacancy centers in diamond. *Applied Physics Letters* **99**(16), 161903 (2011).
 - [12] Schirhagl, R., Chang, K., Loretz, M., and Degen, C. L. Nitrogen-vacancy centers in diamond: nanoscale sensors for physics and biology. *Annual review of physical chemistry* **65**, 83–105 (2014).
 - [13] Kolkowitz, S., Jayich, A. C. B., Unterreithmeier, Q. P., Bennett, S. D., Rabl, P., Harris, J., and Lukin, M. D. Coherent sensing of a mechanical resonator with a single-spin qubit. *Science* **335**(6076), 1603–1606 (2012).
 - [14] Arcizet, O., Jacques, V., Siria, A., Poncharal, P., Vincent, P., and Seidelin, S. A single nitrogen-vacancy defect coupled to a nanomechanical oscillator. *Nature Physics* **7**(11), 879–883 (2011).
 - [15] Yin, Z.-q., Li, T., Zhang, X., and Duan, L. Large quantum superpositions of a levitated nanodiamond through spin-optomechanical coupling. *Physical Review A* **88**(3), 033614 (2013).
 - [16] Scala, M., Kim, M., Morley, G., Barker, P., and Bose, S. Matter-wave interferometry of a levitated thermal nanoscillator induced and probed by a spin. *Physical review letters* **111**(18), 180403 (2013).
 - [17] Romero-Isart, O., Pflanzner, A. C., Blaser, F., Kaltenbaek, R., Kiesel, N., Aspelmeyer, M., and Cirac, J. I. Large quantum superpositions and interference of massive nanometer-sized objects. *Physical review letters* **107**(2), 020405 (2011).
 - [18] Albrecht, A., Retzker, A., and Plenio, M. B. Testing quantum gravity by nanodiamond interferometry with nitrogen-vacancy centers. *Physical Review A* **90**(3), 033834 (2014).
 - [19] Zhao, N. and Yin, Z.-q. Room-temperature ultrasensitive mass spectrometer via dynamical decoupling. *Physical Review A* **90**(4), 042118 (2014).
 - [20] Romero-Isart, O., Juan, M. L., Quidant, R., and Cirac, J. I. Toward quantum superposition of living organisms. *New Journal of Physics* **12**(3), 033015 (2010).
 - [21] Chang, D. E., Regal, C., Papp, S., Wilson, D., Ye, J., Painter, O., Kimble, H. J., and Zoller, P. Cavity optomechanics using an optically levitated nanosphere. *Proceedings of the National Academy of Sciences* **107**(3), 1005–1010 (2010).
 - [22] Geraci, A. A., Papp, S. B., and Kitching, J. Short-range force detection using optically cooled levitated microspheres. *Physical review letters* **105**(10), 101101 (2010).
 - [23] Li, T., Kheifets, S., and Raizen, M. G. Millikelvin cooling of an optically trapped microsphere in vacuum. *Nature Physics* **7**(7), 527–530 (2011).
 - [24] Gieseler, J., Deutsch, B., Quidant, R., and Novotny, L. Subkelvin parametric feedback cooling of a laser-trapped nanoparticle. *Physical review letters* **109**(10), 103603 (2012).
 - [25] Horowitz, V. R., Alemán, B. J., Christle, D. J., Cleland, A. N., and Awschalom, D. D. Electron spin resonance of nitrogen-vacancy centers in optically trapped nanodiamonds. *Proceedings of the National Academy of Sciences* **109**(34), 13493–13497 (2012).
 - [26] Geiselmann, M., Juan, M. L., Renger, J., Say, J. M., Brown, L. J., De Abajo, F. J. G., Koppens, F., and Quidant, R. Three-dimensional optical manipulation of a single electron spin. *Nature nanotechnology* **8**(3), 175–179 (2013).
 - [27] Neukirch, L. P., Gieseler, J., Quidant, R., Novotny, L., and Nick Vamivakas, A. Observation of nitrogen vacancy photoluminescence from an optically levitated nanodiamond. *Optics letters* **38**(16), 2976–2979 (2013).
 - [28] Neukirch, L. P., von Haartman, E., Rosenholm, J. M., and Vamivakas, A. N. Multi-dimensional single-spin nano-optomechanics with a levitated nanodiamond. *Nature Photonics* **9**(10), 653–657 (2015).
 - [29] Toyli, D. M., Christle, D. J., Alkauskas, A., Buckley, B. B., Van de Walle, C. G., and Awschalom, D. D. Measurement and control of single nitrogen-vacancy center spins above 600 k. *Phys. Rev. X* **2**, 031001, Jul (2012).
 - [30] McGuinness, L., Hall, L., Stacey, A., Simpson, D., Hill, C., Cole, J., Ganesan, K., Gibson, B., Praver, S., Mulvaney, P., et al. Ambient nanoscale sensing with single spins using quantum decoherence. *New Journal of*

- Physics* **15**(7), 073042 (2013).
- [31] Steinert, S., Ziem, F., Hall, L., Zappe, A., Schweikert, M., Götz, N., Aird, A., Balasubramanian, G., Hollenberg, L., and Wrachtrup, J. Magnetic spin imaging under ambient conditions with sub-cellular resolution. *Nature communications* **4**, 1607 (2013).
- [32] Li, T., Kheifets, S., Medellin, D., and Raizen, M. G. Measurement of the instantaneous velocity of a brownian particle. *Science* **328**(5986), 1673–1675 (2010).
- [33] Millen, J., Deesuwana, T., Barker, P., and Anders, J. Nanoscale temperature measurements using non-equilibrium brownian dynamics of a levitated nanosphere. *Nature nanotechnology* **9**(6), 425–429 (2014).
- [34] Gieseler, J., Quidant, R., Dellago, C., and Novotny, L. Dynamic relaxation of a levitated nanoparticle from a non-equilibrium steady state. *Nature nanotechnology* **9**(5), 358–364 (2014).
- [35] Lai, N. D., Faklaris, O., Zheng, D., Jacques, V., Chang, H., Roch, J., and Treussart, F. Quenching nitrogen–vacancy center photoluminescence with an infrared pulsed laser. *New Journal of Physics* **15**(3), 033030 (2013).
- [36] Aslam, N., Waldherr, G., Neumann, P., Jelezko, F., and Wrachtrup, J. Photo-induced ionization dynamics of the nitrogen vacancy defect in diamond investigated by single-shot charge state detection. *New Journal of Physics* **15**(1), 013064 (2013).
- [37] Geiselmann, M., Marty, R., de Abajo, F. J. G., and Quidant, R. Fast optical modulation of the fluorescence from a single nitrogen-vacancy centre. *Nature Physics* **9**(12), 785–789 (2013).
- [38] Iakubovskii, K., Adriaenssens, G., and Nesladek, M. Photochromism of vacancy-related centres in diamond. *Journal of Physics: Condensed Matter* **12**(2), 189 (2000).
- [39] Kupriyanov, I., Gusev, V., Pal’yanov, Y. N., and Borzdov, Y. M. Photochromic effect in irradiated and annealed nearly iia type synthetic diamond. *Journal of Physics: Condensed Matter* **12**(35), 7843 (2000).
- [40] Manson, N. and Harrison, J. Photo-ionization of the nitrogen-vacancy center in diamond. *Diamond and related materials* **14**(10), 1705–1710 (2005).
- [41] Fuchs, G., Dobrovitski, V., Toyli, D., Heremans, F., Weis, C., Schenkel, T., and Awschalom, D. Excited-state spin coherence of a single nitrogen-vacancy centre in diamond. *Nature Physics* **6**(9), 668–672 (2010).
- [42] Cole, J. H. and Hollenberg, L. C. Scanning quantum decoherence microscopy. *Nanotechnology* **20**(49), 495401 (2009).
- [43] Xu, N., Chen, J., and Deng, S. Effect of heat treatment on the properties of nano-diamond under oxygen and argon ambient. *Diamond and Related Materials* **11**(2), 249–256 (2002).
- [44] Wolcott, A., Schiros, T., Trusheim, M. E., Chen, E. H., Nordlund, D., Diaz, R. E., Gaathon, O., Englund, D., and Owen, J. S. Surface structure of aerobically oxidized diamond nanocrystals. *The Journal of Physical Chemistry C* **118**(46), 26695–26702 (2014).
- [45] Hausmann, B., Bulu, I., Venkataraman, V., Deotare, P., and Lončar, M. Diamond nonlinear photonics. *Nature Photonics* **8**(5), 369–374 (2014).
- [46] Davies, G. and Hamer, M. Optical studies of the 1.945 eV vibronic band in diamond. In *Proceedings of the Royal Society of London A: Mathematical, Physical and Engineering Sciences*, volume 348, 285–298. The Royal Society, (1976).
- [47] Rogers, L., Armstrong, S., Sellars, M., and Manson, N. Infrared emission of the NV centre in diamond: Zeeman and uniaxial stress studies. *New Journal of Physics* **10**(10), 103024 (2008).
- [48] Ma, Y., Rohlfing, M., and Gali, A. Excited states of the negatively charged nitrogen-vacancy color center in diamond. *Physical Review B* **81**(4), 041204 (2010).
- [49] Plakhotnik, T. and Gruber, D. Luminescence of nitrogen-vacancy centers in nanodiamonds at temperatures between 300 and 700 K: perspectives on nanothermometry. *Physical Chemistry Chemical Physics* **12**(33), 9751–9756 (2010).
- [50] Aspelmeyer, M., Kippenberg, T. J., and Marquardt, F. Cavity optomechanics. *Reviews of Modern Physics* **86**(4), 1391 (2014).
- [51] Berg-Sørensen, K. and Flyvbjerg, H. Power spectrum analysis for optical tweezers. *Review of Scientific Instruments* **75**(3), 594–612 (2004).
- [52] Beresnev, S., Chernyak, V., and Fomyagin, G. Motion of a spherical particle in a rarefied gas. part 2. drag and thermal polarization. *Journal of Fluid Mechanics* **219**, 405–421 (1990).
- [53] Maxwell, J. C. On the dynamical theory of gases. *Philosophical transactions of the Royal Society of London*, 49–88 (1867).
- [54] Sutherland, W. Lii. the viscosity of gases and molecular force. *The London, Edinburgh, and Dublin Philosophical Magazine and Journal of Science* **36**(223), 507–531 (1893).
- [55] Van Oort, E., Manson, N., and Glasbeek, M. Optically detected spin coherence of the diamond NV centre in its triplet ground state. *Journal of Physics C: Solid State Physics* **21**(23), 4385 (1988).
- [56] Lai, N. D., Zheng, D., Jelezko, F., Treussart, F., and Roch, J.-F. Influence of a static magnetic field on the photoluminescence of an ensemble of nitrogen-vacancy color centers in a diamond single-crystal. *Applied Physics Letters* **95**(13), 133101 (2009).
- [57] Doherty, M. W., Struzhkin, V. V., Simpson, D. A., McGuinness, L. P., Meng, Y., Stacey, A., Karle, T. J., Hemley, R. J., Manson, N. B., Hollenberg, L. C., et al. Electronic properties and metrology applications of the diamond NV- center under pressure. *Physical review letters* **112**(4), 047601 (2014).